Journal of Applied Physics | ARTICLE | pubs.aip.org/aip/jap

Light-trapping structures fabricated *in situ* for ultrathin III-V solar cells

Cite as: J. Appl. Phys. **134**, 135307 (2023); doi: 10.1063/5.0160559
Submitted: 2 June 2023 · Accepted: 19 September 2023 ·
Published Online: 5 October 2023 · Corrected: 11 October 2023

Allison N. Perna,[1] Kevin L. Schulte,[2] John Simon,[2] Anna K. Braun,[1] David R. Diercks,[3] Corinne E. Packard,[1,2] and Aaron J. Ptak[2,a)]

AFFILIATIONS

[1] Department of Metallurgy and Materials Engineering, Colorado School of Mines, Golden, Colorado 80401, USA
[2] National Renewable Energy Laboratory, 15013 Denver West Parkway, Golden, Colorado 80401-3305, USA
[3] Shared Instrumentation Facility, Colorado School of Mines, Golden, Colorado 80401, USA

[a)] **Author to whom correspondence should be addressed:** aaron.ptak@nrel.gov

ABSTRACT

Here, we describe a fully *in situ* method of fabricating light-scattering structures on III-V materials that generates a rough morphology via vapor phase etching and redeposition. Fully *in situ* methods support higher industrial throughput by utilizing the growth reactor to generate the light-trapping structures after device growth without removal from the reactor. We use HCl and PH_3 to etch and redeposit scattering morphologies on $Ga_{0.5}In_{0.5}P$ in a dynamic hydride vapor phase epitaxy (D-HVPE) reactor. We show that the addition of PH_3 leads to redeposition during the vapor phase HCl etching of $Ga_{0.5}In_{0.5}P$ and that HCl flow rate and time exposed to HCl-PH_3 each independently cause a linear increase in the redeposited feature size, indicating that redeposition proceeds by island growth in a III-Cl-limited, hydride-enhanced HVPE regime. Auger electron spectroscopy and scanning transmission electron microscopy with energy dispersive spectroscopy (STEM-EDS) reveal redeposition to be highly Ga-rich GaInP, i.e., Ga(In)P. The Ga-rich nature of the redeposition results from the higher thermodynamic driving force for Ga incorporation than for In during HVPE growth and the difference in the volatility of the III-Cl etch products. The resulting morphologies have high broadband scattering, as determined by normal specular reflectance and integrating sphere measurements, indicating effectiveness as light-scattering structures. In a 270-nm-thick GaAs photovoltaic device with a textured back surface, we achieve a 4.9% increase in short circuit current density (J_{SC}) without any loss in open-circuit voltage (V_{OC}) relative to a planar control using only a 60 s *in situ* texturing treatment.

© *2023 Author(s). All article content, except where otherwise noted, is licensed under a Creative Commons Attribution (CC BY) license (http://creativecommons.org/licenses/by/4.0/).* https://doi.org/10.1063/5.0160559

21 November 2023 22:16:30

I. INTRODUCTION

III-V solar cells exhibit the highest conversion efficiencies across all photovoltaic technologies, with single junction GaAs devices boasting over 29% efficiency at one-Sun illumination.[1] Numerous benefits can be realized by thinning the GaAs absorber in so-called ultrathin solar cells, which have approximately a tenfold reduction in thickness compared to conventional solar cells;[2] for single junction III-V photovoltaics, ultrathin means absorber thicknesses below approximately 400 nm. This thinner absorber offers high radiation tolerance[3] and high specific power (W/kg),[4] motivating ultrathin III-V photovoltaic use in space applications. Thinner absorbers also have reduced material use and correspondingly shorter deposition times, which may lower the high cost of III-V epitaxy[5] and support industrial production.[2] Lower manufacturing cost may help expand the market for III-V solar cells to include terrestrial applications where high efficiency and high specific power are paramount.[5] In terms of performance, the open circuit voltage (V_{OC}) increases in thin GaAs solar cells because their smaller volume reduces the diffusion recombination current[6] and their effective photon recycling concentrates light in a smaller volume, increasing carrier density and V_{OC}.[6,7]

The high efficiency and high specific power of III-V solar cells is possible because III-V materials have direct bandgaps leading to strong optical absorption. Ultrathin photovoltaic cells, however, have significant optical transmission losses and correspondingly have a greatly reduced short circuit current density (J_{SC}). Light-trapping schemes are necessary to increase light absorption

© Author(s) 2023

and J_{SC}; in III-V solar cells, these include periodic structures with sharp optical resonances,[8–11] quasi-random structures with slightly broader optical resonances,[12] and random structures with broadband scattering.[13,14] Periodic structures, i.e., photonic crystals, can greatly increase J_{SC} in ultrathin III-V solar cells, but this method requires precise tuning of the photonic crystal structure dimensions that is often achieved with complex and expensive lithographic techniques. Quasi-random photonic crystals do not require such high precision and have been fabricated with polymer blend lithography combined with wet chemical etching.[12] An even simpler method of fabricating light-trapping structures, though, is maskless wet chemical etching to produce rough diffuse scattering morphologies.[13,14] In these techniques, the back surface of the cell is chemically roughened then a metal is deposited to form a textured mirror. Although polymer blend lithography and simple wet chemical etching eliminate the need for highly precise and high-cost photolithography, these methods still require *ex situ* processing with additional capital equipment.

In contrast, light-trapping structures could be fabricated *in situ* using existing capital equipment, i.e., a growth reactor, potentially supporting high industrial throughput. Broadband diffuse scatterers have been fabricated with fully *in situ* methods including vapor phase etching[15] and rough epitaxial growth,[16–18] and both broadband scatterers[15] and photonic crystals[19] have been fabricated with a combination of *ex situ* and *in situ* methods. Vapor phase etching is the *in situ* analog to maskless wet chemical etching, and this method was reported using an unspecified etchant in an organometallic vapor phase epitaxy (OMVPE) reactor to roughen the GaAs back contact layer in a 1 eV InGaAs solar cell.[15] Rough epitaxial growth of AlInP in OMVPE has been demonstrated to increase J_{SC}; however, growth of multiple microns of AlInP was required to achieve sufficient roughening.[17,18] Lattice-mismatched rough growth of 500 nm of GaP has been used to achieve a 6.7% increase in J_{SC} for a solar cell with a 300-nm-thick GaAs absorber, but additional lithographic fabrication was required to contact the back of these devices.[16]

In this work, we describe a fully *in situ* method of texturing the rear contact layer of an inverted ultrathin GaAs solar cell that utilizes *in situ* vapor phase etching and subsequent redeposition of high bandgap Ga(In)P to fabricate a rough, diffuse light-scattering morphology. Unlike other etching-based texturing techniques, this method reclaims a fraction of the etched material for the scattering morphology. In contrast to *in situ* texturing methods that require the fabrication of local vias through the rough scattering surface for back contact metallization,[16] the redeposited scattering morphology inherently contains local vias that enable direct metallization onto the rear surface, although further research on the efficacy of directly contacting the rough morphology is necessary. We perform both the material growth and *in situ* texturing in a dynamic hydride vapor phase epitaxy (D-HVPE) reactor without removing the as-grown sample from the reactor. In the D-HVPE process, texturing is simply an additional step because the required gases, HCl and PH_3, are inherently part of the HVPE process, making HVPE a natural growth technique in which to implement this texturing method; however, this process may be applied in other systems, such as OMVPE. Additionally, because D-HVPE is a high throughput and potentially lower-cost epitaxial growth technique, combining D-HVPE with a fully *in situ* texturing method further supports III-V industrial throughput. We first determine how the resulting textured morphology is affected by the exposure time to the texturing gases, HCl and PH_3, and by the HCl flow rate for constant exposure time. We provide compositional analysis of the textured surface, then explain the physical mechanisms causing the observed composition and rough morphology. We then examine the light-trapping potential of the different resulting morphologies and implement one promising condition into a 270-nm-thick single junction GaAs photovoltaic cell. This textured cell with only a 60 s *in situ* texturing treatment shows a 4.9% improved J_{SC} compared to a device of the same cell structure with a planar back reflector, without any loss in open circuit voltage (V_{OC}).

II. EXPERIMENTAL

Samples were grown in a dual-growth-chamber, atmospheric pressure, D-HVPE reactor described previously.[20] All samples were grown at 650 °C on n-type (100)-oriented GaAs:Si substrates with a 6° offcut toward (111) A. Single junction GaAs solar cells with the rear-heterojunction structure were grown in an inverted fashion as shown in Fig. 1. Inverted cell growth enables *in situ* texturing of the rear surface immediately following growth without removal of the sample from the reactor and without requiring subsequent growth on a roughened surface. The final $Ga_{0.5}In_{0.5}P$:Zn layer, which serves as both the emitter and roughened back contact of the device, was grown thicker in the textured devices to account for vertical etching such that the final planar and textured structures had similar layer thicknesses, aside from the textured morphology. Etching and texturing experiments were performed on $Ga_{0.5}In_{0.5}P$ epilayers grown with the same conditions as the $Ga_{0.5}In_{0.5}P$ emitter/contact layer.

After growth, a large area Au back contact was electroplated directly onto the as-grown, i.e., planar, or textured rear surface using standard processing conditions. The gold adheres roughly conformally on the textured morphology, as confirmed by cross-sectional scanning electron microscopy (SEM) (not shown), forming a textured mirror. Devices with 0.25 cm^2 active area were processed using

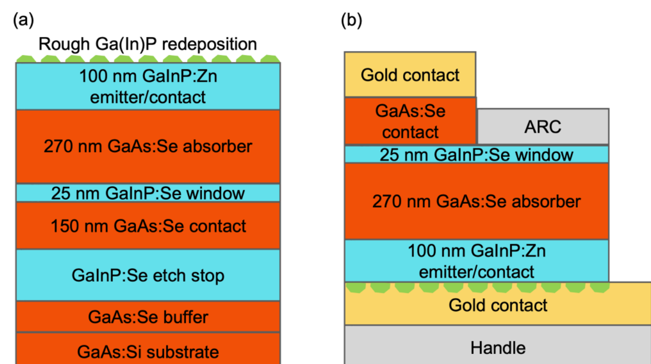

FIG. 1. Cell schematics of the (a) as-grown inverted cell structure and (b) processed cell structure with nominal layer thicknesses.

21 November 2023 22:16:30

© Author(s) 2023

inverted processing techniques.[21] An MgF_2/ZnS/MgF_2 antireflection coating with nominal thicknesses of 96 nm/47 nm/1 nm was deposited.

In a multi-chamber D-HVPE reactor, the growth of a layer proceeds in one chamber while process gases for the next layer are established in the subsequent chamber. During the growth of the rear emitter/contact layer, the adjacent growth chamber is prepared with either HCl or with HCl and PH_3, depending on the experiment. All etching and texturing of $Ga_{0.5}In_{0.5}P$ layers was done immediately after growth without sample removal from the reactor. The control sample for etching and texturing experiments is an as-grown $Ga_{0.5}In_{0.5}P$ epilayer that was removed from the reactor after growth. In etching experiments, HCl was supplied at a flow rate, Q_{HCl}, of 4 SCCM ($P_{HCl} = 0.0008$ atm). In all texturing experiments, PH_3 was supplied at a constant flow rate of 80 SCCM ($P_{PH3} = 0.0110$ atm) and either the total texturing time (10–120 s) or Q_{HCl} (1–10 SCCM) was varied with all other conditions held constant. The PH_3 gas is supplied with an H_2 carrier gas of 2000 SCCM for all experiments. All experiments were conducted at 650 °C in an H_2 atmosphere at a total H_2 flow of 5250 SCCM.

A. Textured morphology characterization

Textured morphologies were imaged with a JEOL JSM-7000F field emission SEM. Plan-view and cross-sectional images were obtained at multiple magnifications from 5 to 40 k× due to variation in feature size across samples. No effect of magnification on any aspect of the analysis was found. Samples were manually cleaved along ⟨110⟩ for cross-sectional SEM imaging. To determine the mechanisms causing the textured morphology, compositional analysis of the textured surface was performed using plan-view Auger electron spectroscopy (AES) and cross-sectional scanning transmission electron microscopy with energy dispersive spectroscopy (STEM-EDS). AES was performed without any surface cleaning and on a Physical Electronics 710 Auger nanoprobe using a 10 kV, 10 nA primary beam. AES data were processed using MultiPak version 9.6.1.7. High-resolution x-ray diffraction (HRXRD) was additionally used to characterize the as-grown material and the textured morphology.

To evaluate potential light-trapping effectiveness, the normal, specular reflectance was measured from the roughened $Ga_{0.5}In_{0.5}P$ surface using an n&k Analyzer 1700-RT. Light that is scattered at an off-angle is not collected in this setup, therefore a lower normal, specular reflectance indicates higher potential for light-trapping via off-angle scattering. In a solar cell, the roughened $Ga_{0.5}In_{0.5}P$ surface is the back side; therefore, light scattering within the cell active layers will vary somewhat from these measurements. Although absorption is not directly measured, backside normal, specular reflectance is advantageous for rapidly measuring different morphologies and has been previously used to evaluate light-trapping potential with reasonable agreement to subsequent cell current enhancement.[13]

Analysis of features in the textured morphologies was performed using Fiji (ImageJ). The total plan-view area coverage of morphological features was measured using Fiji's threshold feature. The average plan-view area of an individual feature was determined after thresholding. Differentiation between adjacent features was done by performing a distance transform watershed using the MorphoLibJ plugin[22] and through visual inspection. The thickness of the morphological features was measured at 20 approximately evenly spaced positions per image. Multiple images were used per sample for each analysis.

B. Cell characterization

Solar cell devices were characterized with external quantum efficiency (EQE), light current density–voltage (J–V), and total and diffuse reflectivity measurements. EQE was measured with a chopped white light source with a monochromator. Light J–V measurements were taken using an XT-10 solar simulator. The AM1.5G spectrum was approximated using a calibrated single junction GaAs reference solar cell and a calculated spectral mismatch correction factor based on the measured cell's EQE. Total and diffuse reflectivity was performed with a Cary7000 UV–Vis spectrophotometer and an external diffuse reflectance accessory DRA2500 integrating sphere. Reflectivity calibrations were performed with a NIST aluminum specular reflectivity standard. Only the active cell area was illuminated through use of a small spot kit and a 5 mm aperture placed physically adjacent to the cell.

III. RESULTS AND DISCUSSION

A. Fabrication of textured morphology

We first etched samples in the growth reactor using HCl to determine if gaseous HCl, a known GaInP etchant,[23] was sufficient as a roughening agent. $Ga_{0.5}In_{0.5}P$ epilayers exposed to HCl alone ($Q_{HCl} = 4$ SCCM, $P_{HCl} = 0.0008$ atm) remain smooth and have a mirror-like finish. Their morphology is similar to that of an as-grown $Ga_{0.5}In_{0.5}P$ epilayer control sample, as determined by Nomarski optical microscopy (not shown), and their normal, specular reflectance is high, as shown in Fig. 2(a). Reflectance modeling using a 1D transfer matrix method shows decreased $Ga_{0.5}In_{0.5}P$ thickness with increasing etch time [see inset, Fig. 2(a)], indicating that the HCl vapor does etch $Ga_{0.5}In_{0.5}P$ as expected. However, the high normal specular reflectance that is similar to that of the control indicates that, under these conditions, gaseous HCl did not generate a textured surface.

In contrast to the planar etching observed while using only HCl, the addition of PH_3 to the HCl vapor etch led to a rough textured surface with low broadband specular reflectance that is potentially useful as a broadband scatterer. We investigated the effects of exposure time to the HCl-PH_3 gas mixture from 10 to 120 s with the HCl flow rate held constant at 4 SCCM. The normal, specular reflectance of $Ga_{0.5}In_{0.5}P$ epilayers textured in HCl-PH_3 [Fig. 2(b) top] varied with texturing time. There was a small decrease in reflectance at wavelengths shorter than 400 nm after 10 s. After 20 s of texturing, the reflectance decreased significantly over most of the wavelength range. Texturing for at least 30 s yielded lower broadband reflectance, indicating promise for light-trapping. At 60 s, the lowest broadband reflectance was achieved for wavelengths longer than approximately 450 nm, but reflectance increases in this wavelength range with longer etch times. We also investigated the effect of HCl flow rate in the HCl–PH_3 mixture

21 November 2023 22:16:30

© Author(s) 2023

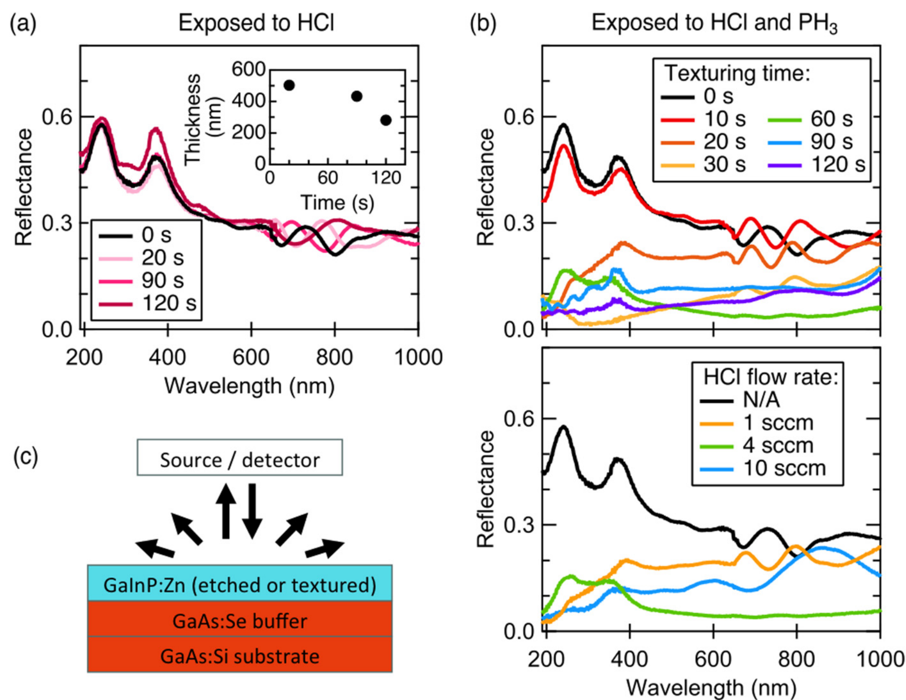

FIG. 2. Normal, specular reflectance of $Ga_{0.5}In_{0.5}P$ epilayers (a) exposed to HCl (Q_{HCl} = 4 sccm, P_{HCl} = 0.0008 atm) for different amounts of time; inset is the modeled remaining epilayer thickness; (b) exposed to HCl-PH_3 (top) for different amounts of time (Q_{HCl} = 4 SCCM, P_{HCl} = 0.0008 atm) and (bottom) for Q_{HCl} from 1 SCCM (P_{HCl} = 0.0002 atm) to 10 SCCM (P_{HCl} = 0.0019 atm) for 60 s. (c) Sample structure and measurement setup.

from 1 to 10 SCCM (P_{HCl} = 0.0002–0.0019 atm) with time held constant at 60 s. There, similarly, was low specular reflectance across a range of HCl flow rates [Fig. 2(b), bottom] with 4 SCCM of HCl providing the lowest reflectance at wavelengths longer than approximately 400 nm.

We investigated the morphology causing the decrease in reflectance using top-down and cross-sectional SEM in Figs. 3 and 4. The SEM images show the development of a rough surface morphology consisting of elevated features with or without an overhang with both texturing time and HCl flow rate, respectively. The approximate boundary between the GaAs buffer layer and the as-grown $Ga_{0.5}In_{0.5}P$ layer was determined with SEM contrast and is marked with a dashed line. The total plan-view area coverage of these features, the average plan-view area of an individual feature, and the average feature thickness all increase linearly with time, as shown in Figs. 3(f)–3(h), respectively. The average plan-view area of an individual feature was not determined for texturing times greater than 60 s because the features become sufficiently interconnected that individual features could not be differentiated. Figures 4(d) and 4(e) show that increasing Q_{HCl} leads to increased plan-view area coverage of elevated features and increased feature thickness, similar to trends observed with increasing texturing time. In both experiments, there appears to be feature elongation along the offcut direction.

Comparing the experiments with different exposure time to HCl–PH_3 and with different Q_{HCl}, we observe that the texturing process is reproducible and that similar morphologies can be achieved under different texturing conditions. One texturing condition similar to both experiments (60 s with a Q_{HCl} of 4 SCCM) was used to produce two different samples shown in Figs. 3(c) and 4(b). The samples have similar normal, specular reflectance, and their morphological features have similar thickness and cover similar plan-view area, demonstrating reproducibility of the texturing process. Similar morphologies with similar broadband reflectance were also achieved when texturing in HCl–PH_3 with Q_{HCl} = 4 SCCM for 20 s [Figs. 3(a) and 2(b) top] and with Q_{HCl} = 1 SCCM for 60 s [Figs. 4(a) and 2(b) bottom]. These observations demonstrate controllability over the texturing process and offer flexibility for growth process optimization. They additionally provide insight into the texturing mechanism, as will be discussed. We also note that the broadband reflectance in Fig. 2(b) for both time and Q_{HCl} experiments has a minimum at longer wavelengths, suggesting that there may be an optimal morphology for minimal broadband normal reflectance over a given wavelength range. However, more work is needed to establish optimal texturing morphologies for implementation into a specific solar cell architecture.

B. Origin of morphology

Our results show that texturing the $Ga_{0.5}In_{0.5}P$ surface can yield different morphologies with varied broadband reflectance. Understanding how these features form is essential toward achieving control over the morphology, and subsequently the reflectance, for the fabrication of effective light-trapping structures. The SEM images alone, however, do not allow us to conclusively identify how the morphology forms. Therefore, we used several measurement techniques to establish the cause of the roughness.

Auger electron spectroscopy (AES) measurements shown in Fig. 5(a) indicate that the features observed in SEM are Ga-rich and In-poor relative to the underlying layer but contain similar amounts of P (not shown). Assuming that the underlying layer is

21 November 2023 22:16:30

© Author(s) 2023

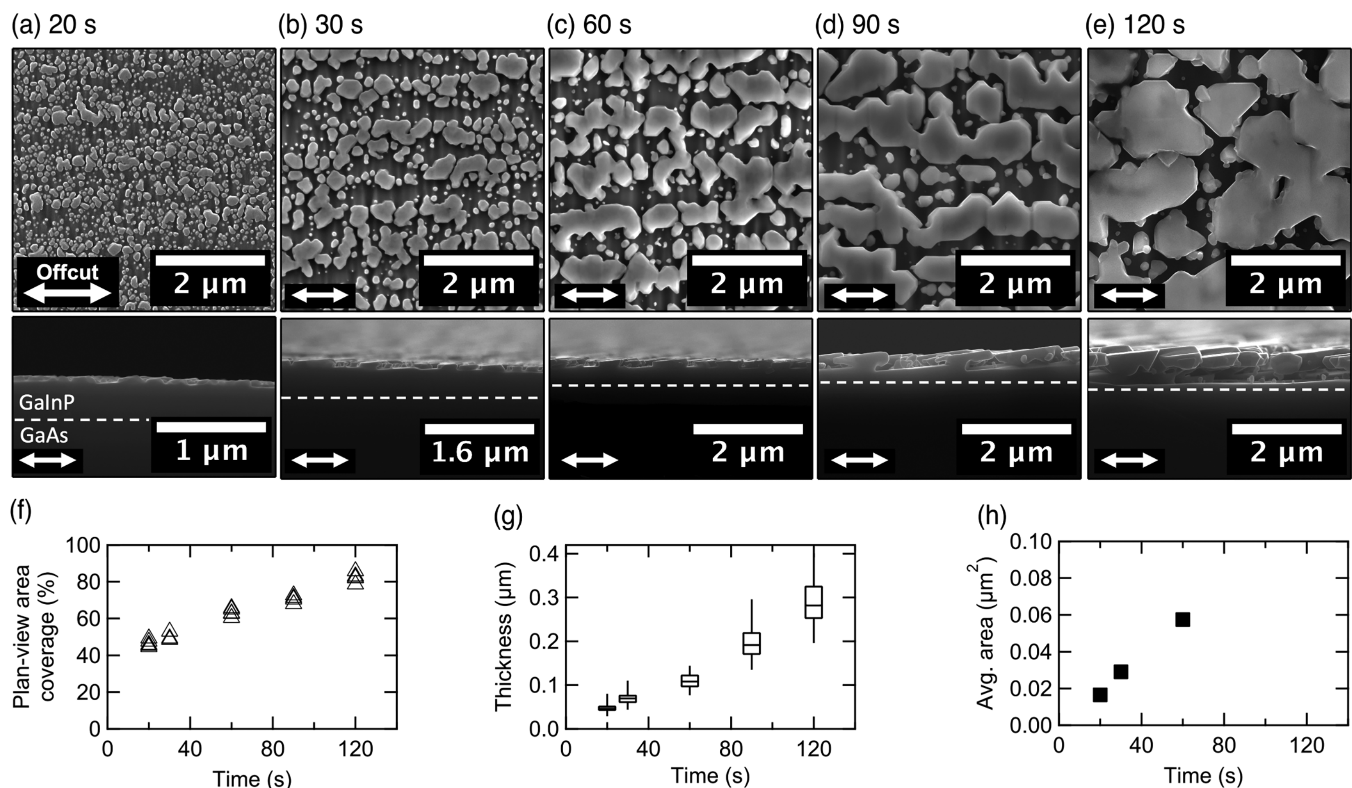

FIG. 3. Plan-view (top) and cross-sectional (bottom) SEM images of $Ga_{0.5}In_{0.5}P$ epilayers textured in HCl-PH_3 (Q_{HCl} = 4 SCCM, P_{HCl} = 0.0008 atm) for (a) 20 s, (b) 30 s, (c) 60 s, (d) 90 s, (e) 120 s. Different data points for a given time represent different images from the same sample. The dashed line marks the approximate demarcation between the GaAs buffer layer and the as-grown $Ga_{0.5}In_{0.5}P$ layer. (f) Total plan-view area coverage of elevated morphological features; (g) average plan-view area of individual elevated features; (h) boxplot of elevated feature thickness showing median and interquartile range. Whiskers show the minimum and maximum values.

21 November 2023 22:16:30

as-grown $Ga_{0.5}In_{0.5}P$, this suggests that the elevated features are Ga-rich $Ga_xIn_{1-x}P$. Figure 5(b) shows cross-sectional STEM-EDS maps through one morphological feature in a sample textured in HCl–PH_3 for 120 s with a Q_{HCl} of 4 SCCM [also shown in Fig. 3(e)]. Figure 5(c) shows EDS line profile data taken through the center of this feature from top to bottom. The Pt signal is due to the deposition of a protective Pt layer during sample preparation. Using the EDS area and line profile data and the high-angle annular dark-field (HAADF) image, we identify three distinct regions in the feature from top to bottom: an elevated GaP-rich feature, an as-grown underlying $Ga_{0.5}In_{0.5}P$ layer showing a remaining "pillar" region, and the as-grown GaAs buffer layer. In both the EDS area maps [Fig. 5(b)] and line profile [Fig. 5(c)], the elevated feature and underlying $Ga_{0.5}In_{0.5}P$ region have similar and homogeneous P signals, and the elevated feature is Ga-rich relative to the underlying layer, in agreement with the AES results. EDS line profile data from the Ga-rich elevated feature are summarized in Table I, providing average values for the GaP-rich shaded region in Fig. 5(c). The table shows both raw signals and recalculated signals that invoke stoichiometry between the group III and group V signals such that the total group III and V signals sum to 50% each. These line profile data indicate that there is approximately 3% In incorporation, on average, in the GaP-rich elevated feature, i.e., a composition of approximately $Ga_{0.94}In_{0.06}P$.

We also performed HRXRD on samples textured from 20 to 120 s shown in Fig. 3 to characterize the composition and strain. Normalized symmetric HRXRD scans shown in Fig. 6 have a primary peak that contains the (004) reflections for the GaAs substrate and as-grown GaAs buffer layer. The as-grown $Ga_{0.5}In_{0.5}P$ (004) peak (see Fig. 6 inset) shows slight lattice mismatch to the substrate and a composition of $Ga_{0.53}In_{0.47}P$, determined using Vegard's law. A tensile-strained peak emerges after 45 s of texturing, increasing in intensity and shifting closer to the substrate peak with increasing texturing time. At 120 s, the peak is positioned at approximately +4400 arcsec with a FWHM of 860 arcsec, corresponding to the same GaInP composition observed in STEM-EDS, $Ga_{0.94}In_{0.06}P$, assuming 100% relaxation in the growth direction. The emergence of this peak with time suggests the growth of new materials with epitaxial registry to the underlying layer. Utilizing the composition data and SEM images in Fig. 3, we conclude that the textured morphology forms via island growth of (001)-oriented Ga-rich GaInP, i.e., Ga(In)P.

© Author(s) 2023

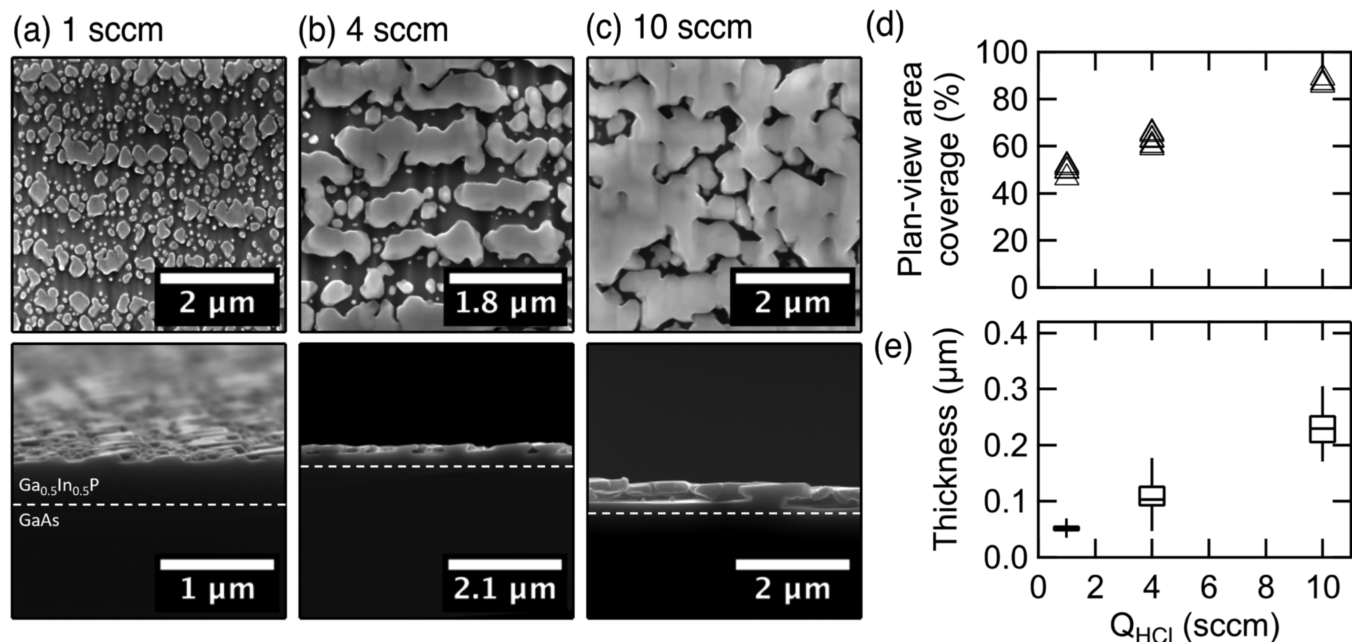

FIG. 4. Plan-view (top) and cross-sectional (bottom) SEM images of $Ga_{0.5}In_{0.5}P$ epilayers textured in HCl-PH_3 for 60 s with (a) Q_{HCl} = 1 SCCM (P_{HCl} = 0.0002 atm), (b) Q_{HCl} = 4 SCCM (P_{HCl} = 0.0008 atm), (c) Q_{HCl} = 10 SCCM (P_{HCl} = 0.0019 atm). Different data points for a given flow rate represent different images from the same sample. The dashed line marks the approximate demarcation between the GaAs buffer layer and the as-grown $Ga_{0.5}In_{0.5}P$ layer. (d) Total plan-view area coverage of elevated morphological features; (e) boxplot of elevated feature thickness showing median and interquartile range. Whiskers show the minimum and maximum values.

The observation that the textured morphology does not form from HCl etching alone (not shown) and does form with supplied PH_3 suggests that redeposition and island growth of Ga(In)P result from reactions between etch products and the supplied PH_3. This phenomenon can be explained by HVPE growth mechanisms. The planar etching observed when only using gaseous HCl likely indicates that the reaction of HCl with $Ga_{0.5}In_{0.5}P$ results in volatile etch products according to the reverse growth reaction in HVPE,

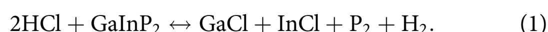

$$2HCl + GaInP_2 \leftrightarrow GaCl + InCl + P_2 + H_2. \quad (1)$$

The presence of metal chlorides and P_x etch products provides the ingredients for a growth reaction; however, redeposition is not observed because Eq. (1) has high thermodynamic and kinetic barriers to growth at the texturing temperature of 650 °C.[24] Growth at 650 °C is possible in the hydride-enhanced HVPE growth regime by a reaction of the form

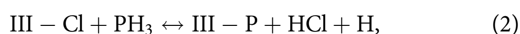

$$III - Cl + PH_3 \leftrightarrow III - P + HCl + H, \quad (2)$$

which has much lower kinetic and thermodynamic barriers to growth than growth from P_x compounds.[24] By supplying PH_3, we enable the redeposition of Ga(In)P that forms the textured morphology.

Compositional data in Figs. 5 and 6 show that redeposition by Eq. (2) is highly Ga-rich, indicating that the majority of the InCl liberated via Eq. (1) is not incorporated in the redeposited solid. This situation likely occurs because GaP growth is more thermodynamically favored than InP growth[25] and InCl has a higher desorption rate than GaCl due to its weak adsorption energy relative to GaCl.[26] To grow $Ga_{0.5}In_{0.5}P$ under typical conditions in our reactor, these mechanisms necessitate a high InCl to GaCl ratio, i.e., >5.[27,28] Thus, we can expect the redeposited solid to be Ga-rich because the HCl-etching of $Ga_{0.5}In_{0.5}P$ liberates InCl and GaCl in a 1:1 ratio. Furthermore, free HCl supplied during growth has been shown to increase the Ga:In ratio in the solid during the growth of other III-V compounds.[29] The presence of free HCl as a reaction product likely further suppresses In incorporation during redeposition by contributing to the HCl partial pressure. Previous literature on *in situ* etching for microfabrication applications similarly reports GaP redeposition in the vapor phase etching of Ga-containing III-V compounds by Cl-based etchants in the presence of supplied PH_3;[30–32] experimental verification of GaP redeposition is provided in Ref. 30.

This redeposition process also explains the trends in increasing feature size with time and Q_{HCl}. Fig. 3 shows that the average feature size and thickness trend toward zero at zero time and have a constant growth rate, indicating island growth starting from nucleation. The plan-view area coverage of these features [Fig. 3(f)] does not trend toward zero because nucleation occurs in numerous places simultaneously after an undetermined time; therefore, there is a rapid trend from zero to a relatively large fraction. Increased feature size and plan-view area coverage with Q_{HCl} (Fig. 4) indicate higher growth rate with Q_{HCl}, which is explained by concurrent

21 November 2023 22:16:30

© Author(s) 2023

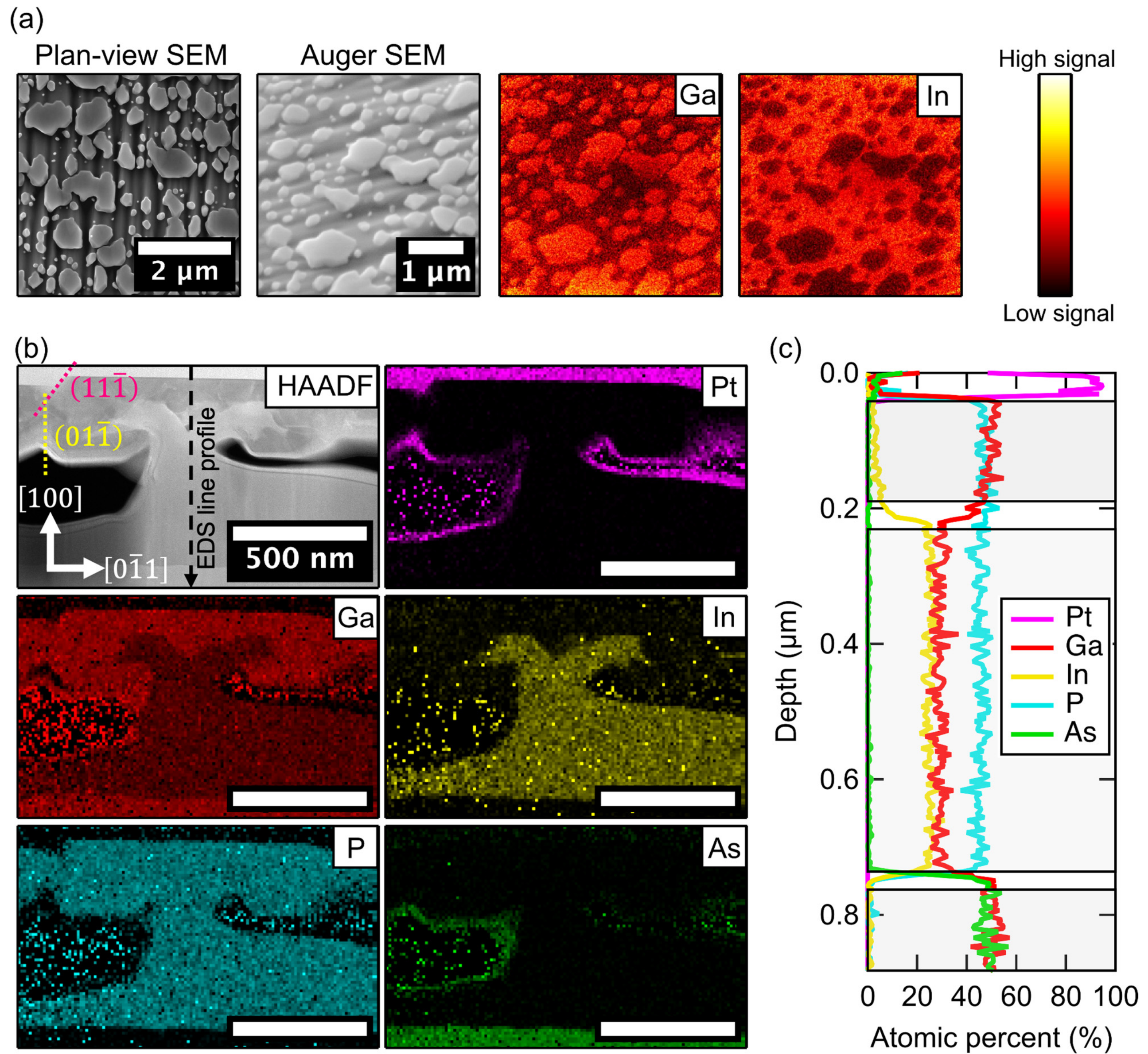

FIG. 5. Compositional characterization of $Ga_{0.5}In_{0.5}P$ epilayers textured in $HCl-PH_3$. (a) Auger electron spectroscopy (AES) showing, from left to right, plan-view SEM image of the sample, SEM image of the sample as imaged during AES, the Ga signal, and the In signal. The sample was textured in $HCl-PH_3$ (Q_{HCl} = 1 SCCM, P_{HCl} = 0.0002 atm) for 120 s; (b) STEM-EDS of one morphological feature of a sample textured in $HCl-PH_3$ (Q_{HCl} = 4 SCCM, P_{HCl} = 0.0008 atm) for 120 s. (c) STEM-EDS line profile taken through the imaged morphological feature.

TABLE I. STEM-EDS line profile data in the GaP-rich elevated region showing atomic percent. Normalized signal is given in parenthesis. The reported error is the standard deviation in atomic percent of the mean composition in this region.

Layer	at. % Ga	at. % In	at. % As	at. % P
Top (Ga(In)P)	49.4 ± 2.7 (47.1 ± 2.6)	3.1 ± 1.6 (2.9 ± 1.5)	0.2 ± 0.1 (0.2 ± 0.1)	47.3 ± 0.5 (49.8 ± 0.6)
Middle ($Ga_{0.5}In_{0.5}P$)	28.9 ± 1.1 (26.6 ± 1.0)	25.4 ± 8.4 (23.4 ± 7.7)	0.2 ± 0.1 (0.3 ± 0.1)	45.5 ± 0.3 (49.7 ± 0.4)
Bottom (GaAs)	50.0 ± 2.1 (49.1 ± 2.1)	0.9 ± 0.5 (0.9 ± 0.5)	48.4 ± 1.0 (49.3 ± 1.0)	0.7 ± 0.1 (0.7 ± 0.1)

21 November 2023 22:16:30

© Author(s) 2023

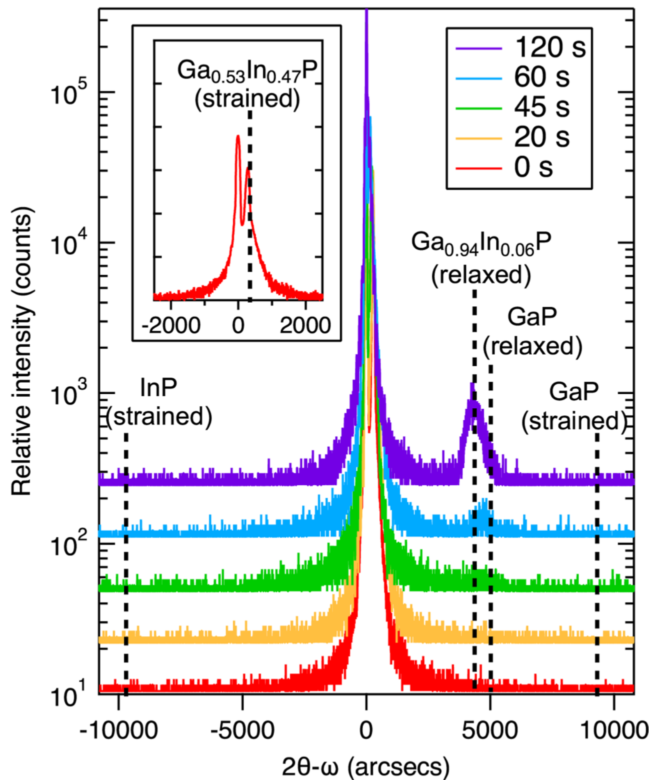

FIG. 6. Normalized $2\theta-\omega$ scans of $Ga_{0.5}In_{0.5}P$ epilayers textured in HCl-PH_3 (Q_{HCl} = 4 SCCM, P_{HCl} = 0.0008 atm) for different amounts of time from 0 to 120 s. Vertical lines indicate expected positions of various $Ga_xIn_{1-x}P$ compositions with out-of-plane relaxation state indicated in parentheses: "relaxed" indicates 100% relaxation and "strained" indicates 0% relaxation. The inset is the normalized $2\theta-\omega$ scan of the 0 s control.

HCl-limited etching and group III metal chloride (III-Cl) limited growth mechanisms. Increasing Q_{HCl} in an HCl-limited etch regime increases the amount of etching of as-grown $Ga_{0.5}In_{0.5}P$ via Eq. (1), which generates a higher partial pressure of III-Cl etch products near the surface. In a III-Cl limited growth regime, increasing the partial pressure of the metal chlorides will increase the redeposition growth rate by Eq. (2).

It is possible that a ripening process contributes to the increase in average Ga(In)P feature size with time. Ripening is a temperature-induced process by which metal chlorides diffuse either through the vapor or by surface diffusion from smaller Ga(In)P features to larger features and would occur even in the absence of the supplied HCl and PH_3. To determine if ripening contributes significantly to particle growth, we textured a sample for 30 s in one chamber then annealed it in the adjacent chamber for 30 s under PH_3 at the texturing temperature, 650 °C. We compared this sample to samples textured using the same conditions for either 30 or 60 s without the subsequent anneal step. Plan-view SEM images in Fig. 7 show that the sample textured for 30 s then annealed for 30 s [Fig. 7(b)] has similar morphology as the 30 s textured, non-annealed sample [Fig. 7(a)], which is notably different from the 60 s texture sample [Fig. 7(c)] morphology. This indicates that Ga(In)P feature growth is primarily from the redeposition of etch products and not from ripening processes.

C. Redeposition growth progression

The Ga(In)P crystalline features shown in cross section in Fig. 3 and Fig. 4 have a (100) vertical face inclined to the surface by 6° in the direction of the intentional substrate offcut and some lateral faces corresponding to {110} and {111}-type planes, as shown in the cross-sectional HAADF image in Fig. 5(b). The 6° (100) surface inclination matches the degree of substrate offcut, and SEM images comparing the distance from the as-grown $Ga_{0.5}In_{0.5}P$/GaAs interface to the (100) Ga(In)P surface show minimal vertical growth along [100]. The surface does not begin step-free; however, step-flow growth may be self-limiting on the island faces, forming the exact (100) surface at an inclination matching the intentional substrate offcut. The step-free (100) surface would promote high surface diffusion such that impinging etch products laterally diffuse to the edges of the feature and grow along the sidewalls, effectively inhibiting vertical growth. The stable {110} and {111} facets formed in this way continue to grow laterally, both from impinging atoms that land on the facets and from material that diffuses from the passive (100) surface, until they begin to coalesce with neighboring features. The Ga(In)P features appear elongated in the [011] and $[0\bar{1}\bar{1}]$ directions. This may be

21 November 2023 22:16:30

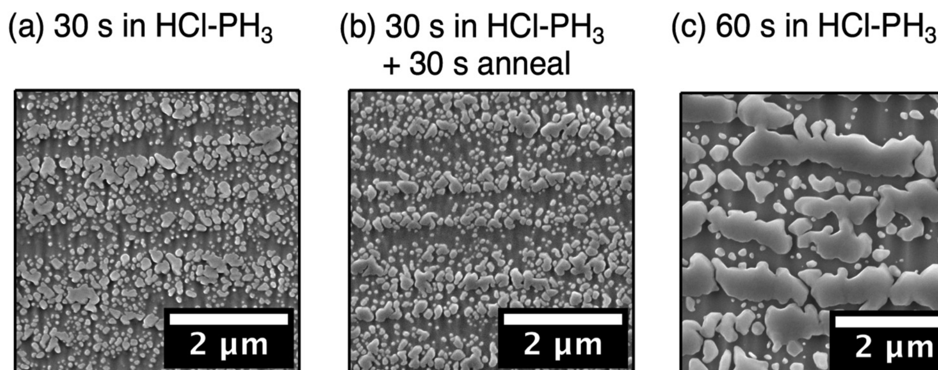

FIG. 7. Plan-view SEM images of samples textured in HCl-PH_3 (Q_{HCl} = 4 SCCM, P_{HCl} = 0.0008 atm) for (a) 30 s, (b) 30 s then annealed under PH_3 for 30 s, (c) 60 s, showing no significant increase in Ga(In)P feature size due to ripening.

© Author(s) 2023

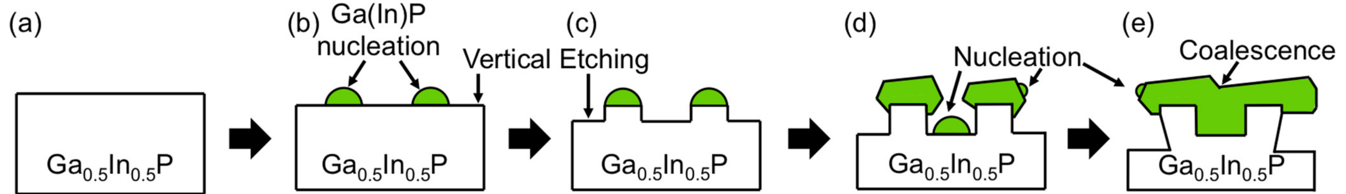

FIG. 8. Schematic of the texturing process in cross section. The sample is continuously exposed to HCl and PH_3. (a) As-grown $Ga_{0.5}In_{0.5}P$; (b) HCl-etching of $Ga_{0.5}In_{0.5}P$ and nucleation of Ga(In)P islands from etch products and PH_3; (c) Ga(In)P masks the vertical HCl-etching of $Ga_{0.5}In_{0.5}P$; (d) Ga(In)P islands evolve and grow to exact (100) ,{111}, and {110} planes; (e) Ga(In)P islands coalesce and HCl laterally etches $Ga_{0.5}In_{0.5}P$ pillars.

due to the substrate offcut, which is along the $[0\bar{1}\bar{1}]$ direction. Lateral growth on the {111} faces may also be faster on {111} A than {111} B, which has been observed in the HVPE growth of GaAs.[33]

Figure 8 presents a schematic representation of the process described above. (a) HCl chemically etches $Ga_{0.5}In_{0.5}P$, liberating InCl and GaCl via Eq. (1). The etching process continues throughout each subsequent step. (b) Liberated metal chlorides and supplied PH_3 react via Eq. (2) causing Ga(In)P island nucleation on the etched $Ga_{0.5}In_{0.5}P$ surface. The redeposition has epitaxial registry with the underlying $Ga_{0.5}In_{0.5}P$. (c) Redeposited Ga(In)P islands act as an etch mask to vertical HCl etching of as-grown $Ga_{0.5}In_{0.5}P$. (d) Ga(In)P islands grow vertically to an exact (100) surface and laterally to various {11n} planes, including {110} and {111}. Throughout etching, new Ga(In)P islands nucleate both homogeneously and heterogeneously. Nucleation and growth may occur within the trench formed between two as-grown $Ga_{0.5}In_{0.5}P$ pillars, forming a morphology similar to what is observed in STEM-EDS [Fig. 5(b)]. (e) The Ga(In)P islands coalesce to form a semi-continuous sheet. HCl etches $Ga_{0.5}In_{0.5}P$ vertically and laterally, attacking the $Ga_{0.5}In_{0.5}P$ "pillars" below the Ga(In)P features as well as the underlying as-grown $Ga_{0.5}In_{0.5}P$ lateral layer. This process results in both the shape and material compositions observed in these features, such as the feature shown in Fig. 5(b).

D. Solar cell performance

In this section, we demonstrate a textured solar cell with increased current density over a planar control and show that the increased current density is due to light-scattering from the rough surface. One texturing condition that produces a scattering morphology with low broadband specular reflectance is texturing in HCl–PH_3 for 60 s with a Q_{HCl} of 4 SCCM (P_{HCl} = 0.0008 atm). We implemented this condition into a 270 nm-thick rear heterojunction (RHJ) GaAs solar cell and compared its performance with a planar control cell of the same thickness without texturing.

Figure 9(a) shows current density–voltage measurements of the best performing textured and planar solar cells and Table II shows performance metrics of the four total devices per sample. The best performing 270-nm-thick textured cell has a J_{SC} of 21.84 mA/cm^2, achieving a 4.9% increase in J_{SC} relative to the best performing planar control. The average increase in current density in the textured sample across all devices is 5.1%. The textured cell has a similar EQE at all wavelengths as the control cell, shown in

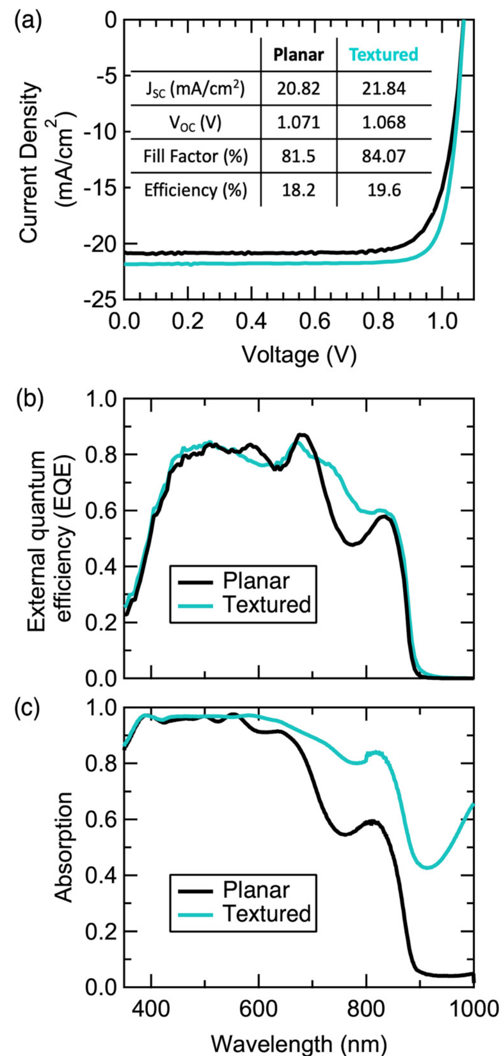

FIG. 9. Cell measurements of thin solar cells without texturing (black) and textured (blue) in HCl-PH_3 with a Q_{HCl} of 4 SCCM for 60 s); (a) Current density vs voltage; (b) External quantum efficiency; (c) Absorption calculated as $A = 1–R_h$ with total hemispherical reflectance, R_h, obtained from UV-Vis with an integrating sphere.

21 November 2023 22:16:30

© Author(s) 2023

TABLE II. Average and standard deviation of current density–voltage performance metrics of planar and textured solar cells with four devices per sample. Performance of selected device is given in parentheses.

	J_{SC} (mA/cm^2)	V_{OC} (V)	FF (%)
HG232 planar	20.69 ± 0.14 (20.82)	1.068 ± 0.008 (1.071)	79.57 ± 2.63 (81.50)
HG215 textured	21.74 ± 0.15 (21.84)	1.061 ± 0.006 (1.068)	77.58 ± 5.50 (84.07)

Fig. 9(b). However, Fabry–Pérot resonances characteristic of planar interfaces in thin film material stacks are reduced in the textured cell, thus increasing J_{SC}. Integrating the EQE of the selected device yields J_{SC} values of 23.3 and 22.1 mA/cm^2 in the textured cell and planar cell, respectively, corresponding to the J_{SC} increase observed in the current density-voltage measurement. There is no appreciable loss in V_{OC} or fill factor, indicating similar material quality and no adverse effect on the back contact metallization, respectively. Due to the limited sample size ($N = 4$), however, further study and optimization is necessary to explore device homogeneity across a full wafer. The resulting textured cell efficiency is 19.6% and the planar cell efficiency is 18.2%.

We determined the total reflectance and absorption of the planar and textured solar cells with UV–Vis reflection measurements using an integrating sphere. The total hemispherical reflectance, R_h, collected in the integrating sphere can be used to calculate total absorption in the device. The rear gold contact is optically thick and adhered to a silicon handle, so we assume there is zero transmission. The total absorption is therefore $A = 1 - R_h$. Figure 9(c) shows that the textured cell displays a significant increase in absorption over the planar cell. This enhanced optical absorption explains why the textured cell has a higher integrated EQE and J_{SC} than the planar control. In an ideal cell without parasitic absorption or recombination, the absorption would be equal to the external quantum efficiency, EQE. We observe a lower EQE than absorption in both cells that, for the textured cell, is more significant at long wavelengths. This may be due to parasitic absorption in the rough gold surface, causing the metal to act as a lossy mirror.[34] Optimization of the rear side metallization process may limit these losses and allow increased current collection.

IV. CONCLUSIONS

We developed a fully *in situ* method of texturing $Ga_{0.5}In_{0.5}P$ to form broadband diffuse scattering structures and demonstrate this method within a dynamic HVPE reactor. We showed through compositional analysis that etching $Ga_{0.5}In_{0.5}P$ in an HCl and PH_3 environment causes Ga(In)P redeposition via hydride-enhanced HVPE growth. The redeposited morphological features are shown to be larger with longer exposure to HCl-PH_3 because there is continuous nucleation and island growth, and features are larger with higher HCl flow rate because redeposition under these conditions operates in a group III-limited growth regime. We textured a 270-nm-thick GaAs rear heterojunction solar cell with a condition that demonstrated high off-angle scattering, yielding a 4.9% boost in J_{SC} without any loss in V_{OC} relative to a planar control, with only a 60 s treatment. This study provides a physical understanding of a III-V etching and redeposition process that can be utilized as an *in situ* and potentially low-cost method of texturing III-V solar cells.

ACKNOWLEDGMENTS

The authors would like to acknowledge David Guiling for materials growth and Evan Wong for device processing. Some of the work was performed in following core facility, which is a part of Colorado School of Mines Shared Instrumentation Facility (Electron Microscopy: RRID:SCR_022048). This work was authored by the National Renewable Energy Laboratory, operated by Alliance for Sustainable Energy, LLC, for the U.S. Department of Energy (DOE) under Contract No. DE-AC36-08GO28308. The information, data, or work presented herein was funded by U.S. Department of Energy, Office of Energy Efficiency and Renewable Energy, Solar Energy Technologies Office under award 38261. The views expressed in the article do not necessarily represent the views of the DOE or the U.S. Government. The U.S. Government retains and the publisher, by accepting the article for publication, acknowledges that the U.S. Government retains a nonexclusive, paid-up, irrevocable, worldwide license to publish or reproduce the published form of this work, or allow others to do so, for U.S. Government purposes. A.N.P. acknowledges support from the U.S. Department of Energy Graduate Assistance in Areas of National Need fellowship. A.K.B. acknowledges support from the National Science Foundation Graduate Research Fellowship Program under Grant No. DGE-1646713. Any opinions, findings, and conclusions or recommendations expressed in this material are those of the authors and do not necessarily reflect the views of the National Science Foundation.

21 November 2023 22:16:30

AUTHOR DECLARATIONS

Conflict of Interest

The authors have no conflicts to disclose.

Author Contributions

Allison N. Perna: Formal analysis (lead); Methodology (lead); Writing – original draft (lead). **Kevin L. Schulte:** Formal analysis (equal); Writing – review & editing (equal). **John Simon:** Formal analysis (equal); Writing – review & editing (equal). **Anna K. Braun:** Writing – review & editing (equal). **David R. Diercks:** Formal analysis (equal). **Corinne E. Packard:** Supervision (equal); Writing – review & editing (equal). **Aaron J. Ptak:** Conceptualization (lead); Supervision (equal); Writing – review & editing (equal).

© Author(s) 2023

DATA AVAILABILITY

The data that support the findings of this study are available from the corresponding author upon reasonable request.

REFERENCES

[1]M. A. Green *et al.*, "Solar cell efficiency tables (Version 57)," Prog. Photovolt. Res. Appl. **29**, 3–15 (2021).
[2]I. Massiot, A. Cattoni, and S. Collin, "Progress and prospects for ultrathin solar cells," Nat. Energy **5**, 959–972 (2020).
[3]L. C. Hirst *et al.*, "Intrinsic radiation tolerance of ultra-thin GaAs solar cells," Appl. Phys. Lett. **109**(3), 033908 (2016).
[4]M. O. Reese *et al.*, "Increasing markets and decreasing package weight for high-specific-power photovoltaics," Nat. Energy **3**(11), 1002–1012 (2018).
[5]K. A. Horowitz, T. W. Remo, B. Smith, and A. J. Ptak, "A Techno-Economic Analysis and Cost Reduction Roadmap for III-V Solar Cells," National Renewable Energy Laboratory (NREL), Golden, CO, NREL/TP-6A20-72103, 2018.
[6]G. Lush and M. Lundstrom, "Thin film approaches for high-efficiency III–V cells," Solar Cells **30**(1–4), 337–344 (1991).
[7]O. D. Miller, E. Yablonovitch, and S. R. Kurtz, "Strong internal and external luminescence as solar cells approach the Shockley–Queisser limit," IEEE J. Photovolt. **2**(3), 303–311 (2012).
[8]H.-L. Chen *et al.*, "A 19.9%-efficient ultrathin solar cell based on a 205-nm-thick GaAs absorber and a silver nanostructured back mirror," Nat. Energy **4**(9), 761–767 (2019).
[9]L. Sayre *et al.*, "Ultra-thin GaAs solar cells with nanophotonic metal-dielectric diffraction gratings fabricated with displacement Talbot lithography," Prog. Photovolt. Res. Appl. **30**(1), 96–108 (2022).
[10]J. Grandidier, D. M. Callahan, J. N. Munday, and H. A. Atwater, "Gallium arsenide solar cell absorption enhancement using whispering gallery modes of dielectric nanospheres," IEEE J. Photovolt. **2**(2), 123 (2012).
[11]S.-M. Lee *et al.*, "High performance ultrathin GaAs solar cells enabled with heterogeneously integrated dielectric periodic nanostructures," ACS Nano **9**(10), 10356–10365 (2015).
[12]J. Buencuerpo *et al.*, "Efficient light-trapping in ultrathin GaAs solar cells using quasi-random photonic crystals," Nano Energy **96**, 107080 (2022).
[13]M. van Eerden *et al.*, "A facile light-trapping approach for ultrathin GaAs solar cells using wet chemical etching," Prog. Photovolt. Res. Appl. **28**(3), 200–209 (2020).
[14]J. R. D'Rozario, S. J. Polly, G. T. Nelson, and S. M. Hubbard, "Thin gallium arsenide solar cells with maskless back surface reflectors," IEEE J. Photovolt. **10**(6), 1681–1688 (2020).
[15]J. D'Rozario, S. J. Polly, S. R. Tatavarti, and S. M. Hubbard, "Light management for improved photon absorption in thin-film radiation-tolerant multijunction space photovoltaics," in *Physics, Simulation, and Photonic Engineering of Photovoltaic Devices XI, San Francisco, March 2022* (SPIE, 2022), p. 11.
[16]D. Woude *et al.*, "Ultrathin GaAs solar cells with a high surface roughness GaP layer for light-trapping application," Prog. Photovolt. Res. Appl. **30**, 622 (2022).
[17]W. Yang *et al.*, "Ultra-thin GaAs single-junction solar cells integrated with a reflective back scattering layer," J. Appl. Phys. **115**(20), 203105 (2014).
[18]J. R. D'Rozario, S. J. Polly, R. Tatavarti, and S. M. Hubbard, "Advancements in light management for thin-film space photovoltaics," in *2021 IEEE 48th Photovoltaic Specialists Conference (PVSC)*, Fort Lauderdale, FL (IEEE, 2021), pp. 1266–1269.
[19]Q. Zheng *et al.*, "Epitaxial growth of three dimensionally structured III-V photonic crystal via hydride vapor phase epitaxy," J. Appl. Phys. **118**(22), 224303 (2015).
[20]D. L. Young, A. J. Ptak, T. F. Kuech, K. Schulte, and J. D. Simon, "High throughput semiconductor deposition system," US10 **192**, 740B2 (2019); available at: https://www.osti.gov/biblio/1499123.
[21]A. Duda, S. Ward, and M. Young, "Inverted metamorphic multijunction (IMM) cell processing instructions," NREL/TP-5200-54049, 1036035, February 2012.
[22]D. Legland, I. Arganda-Carreras, and P. Andrey, "Morpholibj: Integrated library and plugins for mathematical morphology with ImageJ," Bioinformatics **32**(22), 3532–3534 (2016).
[23]A. R. Clawson, "Guide to references on III–V semiconductor chemical etching," Mater. Sci. Eng. R: Rep. **31**(1–6), 1–438 (2001).
[24]K. L. Schulte, A. Braun, J. Simon, and A. J. Ptak, "High growth rate hydride vapor phase epitaxy at low temperature through use of uncracked hydrides," Appl. Phys. Lett. **112**(4), 042101 (2018).
[25]H. Seki and A. Koukitu, "Solid composition of alloy semiconductors grown by MOVPE, MBE, VPE and ALE," J. Cryst. Growth **98**, 118–126 (1989).
[26]A. Usui, "Atomic layer epitaxy," Mat. Res. Soc. Symp. Proc. **198**, 183–193 (1990).
[27]K. L. Schulte, W. Metaferia, J. Simon, and A. J. Ptak, "Uniformity of GaAs solar cells grown in a kinetically-limited regime by dynamic hydride vapor phase epitaxy," Sol. Energy Mater. Sol. Cells **197**, 84–92 (2019).
[28]A. G. Sigai, C. J. Nuese, R. E. Enstrom, and T. Zamerowski, "Vapor growth of In l_ GaP for p-n junction electroluminescence" J. Electrochem. Soc. **120**, 947 (1973).
[29]K. L. Schulte *et al.*, "Metalorganic vapor phase growth of quantum well structures on thick metamorphic buffer layers grown by hydride vapor phase epitaxy," J. Cryst. Growth **370**, 293–298 (2013).
[30]D. Bertone, R. Campi, and G. Morello, "Etching of InP-based MQW laser structure in a MOCVD reactor by chlorinated compounds," J. Cryst. Growth **195**(1–4), 624–629 (1998).
[31]T. Tsuchiya, T. Kitatani, K. Ouchi, H. Sato, and M. Aoki, "*In-situ* etching of InP and InGaAlAs materials by using HCl gas in metalorganic vapor-phase epitaxy," J. Cryst. Growth **272**(1–4), 125–130 (2004).
[32]T. Kitatani, T. Tsuchiya, K. Shinoda, and M. Aoki, "*In situ* etching of InGaAsP/InP by using HCl in an MOVPE reactor," J. Cryst. Growth **274**(3–4), 372–378 (2005).
[33]D. W. Shaw, "Kinetic aspects in vapour phase epitaxy of III V compounds," J. Cryst. Growth **31**, 130–141 (1975).
[34]M. van Eerden, J. van Gastel, G. J. Bauhuis, E. Vlieg, and J. J. Schermer, "Comprehensive analysis of photon dynamics in thin-film GaAs solar cells with planar and textured rear mirrors," Sol. Energy Mater. Sol. Cells **244**, 111708 (2022).

21 November 2023 22:16:30

© Author(s) 2023